Light–controlled hydrogel platform for high-resolution chemical stimulation

Hojjat Rostami Azmand, Youngsik Song, and Sang-Woo Seo

Department of Electrical Engineering, The City College of New York, 160 Convent Avenue, New York, NY 10031, USA Email: swseo@ccny.cuny.edu

Abstract

Localized chemical delivery plays an essential role in the fundamental information transfers within biological systems. Thus, the ability to mimic the natural chemical signal modulation would provide significant contributions to understand the functional signaling pathway of biological cells and develop new prosthetic devices for neurological disorders. In this paper, we demonstrate a light-controlled hydrogel platform that can be used for localized chemical delivery in a high spatial resolution. By utilizing the photothermal behavior of graphene-hydrogel composites confined within micron-sized fluidic channels, patterned light illumination creates the parallel and independent actuation of chemical release in a group of fluidic ports. The new platform promises the feasibility of creating a novel synaptic interface with large arrayed chemical stimulation capability toward biochemically controlled neural prosthesis systems.

Key words: temperature-sensitive hydrogel, photothermal actuation, local chemical delivery, chemical stimulation, macroporous silicon, light actuated chemical release.

1. Introduction

The information transfer at the synapses is mainly through the flux modulations of specific neurotransmitters between neuron cells [1]. To bypass the damaged neurons, neural prosthesis technologies are designed to create artificial interconnections for restoring their functional losses. Traditionally, electrical stimulations that excite neuron cells are successfully applied to restore different sensory functions in our body, including auditory [2] and visual sensing [3, 4], autonomous movement control, and brain stimulation [5, 6]. At the same time, there are also growing interests in mimicking the natural neuron signaling through artificial synaptic interfaces by modulating specific chemical releases [7, 8]. It was reported that the chemical stimulation approaches could overcome limitations of the current electrical stimulation approaches and provide distinct advantages by following chemical-specific responses on a target group of cells [9, 10]. However, typical microfluidics or fluidic transport systems applied to the current chemical stimulations have not been reached at the level of biological complexities due to their limitations in spatial and temporal resolutions. Moreover, typical two-dimensional configuration or bulky setup of the chemical transport systems does not support exciting neuron cells in high spatial resolution and has technological challenges to control large numbers of chemical release in a parallel and independent way.

In this paper, we investigate graphene-hydrogel composites and combine light to control chemical release from a unique three-dimensional (3D) configuration of fluidic release ports. The results provide the feasibility of creating a novel synaptic interface to have a larger array of chemical release control in a parallel and independent way using light. Through our demonstrated approach, it would be possible that an individual or a group of fluidic ports on different locations can release modulated chemicals corresponding to their light actuation.

Utilizing the microfabrication, this new platform can also be easily scalable to accommodate different arrayed configurations without complicating physical interconnections of controlling each port.

2. Design of arrayed fluidic control interface

A macroporous silicon membrane structure (MPS) was devised to form arrayed microfluidic channels through its pores. By embedding graphene mixed temperature-sensitive hydrogel within the pores, the light-actuated chemical release was demonstrated in this paper.

Figure 1(a) shows a schematic of our designed device with a periodic pixel-like array of graphene-hydrogel columns embedded in the pores of an MPS membrane. Figure 1(b) shows a scanning electron microscope image of a macroporous silicon membrane structure. The silicon membrane structure creates an interface between the top chemical release and the bottom chemical reservoir through its arrayed pore channels. The main operational element of the designed interface is a temperature-sensitive hydrogel. Hydrogels are crosslinked polymer networks that are able to absorb large amounts of liquid within their polymer chains, simultaneously leading to matrix shrinkage and expansion without dissolution in liquid by external stimuli actuations including light [11], temperature [12], pH [13], electric field [14], and ultrasound [15]. These unique properties have attracted much attention in various applications in biotechnology, specifically sensing and drug delivery [16-18]. Among different hydrogels, poly-N-isopropyl acrylamide (p-NiPAAm), which is utilized in our structure, has a unique temperature-responsive characteristic at the physiological temperature. When the temperature of the hydrogel increases and passes its volume phase transition temperature (VPTT), the hydrogel becomes hydrophobic and shrinks, leading to the push-out of its stored chemical. On the

contrary, when the temperature of the hydrogel decreases and passes its VPTT [19, 20], it expands and restores its properties. To implement remote temperature actuation using light, we used commercially available graphene nanoplatelets, which have been demonstrated as effective media for converting light energy into heat [21-23]. By dispersing graphene nanoplatelets in p-NiPAAm hydrogel and embedding the hydrogel composite within the pores of the membrane structure, the designed interface structure can control chemical diffusion rate from the bottom reservoir to the top releasing layer remotely by photothermal actuation. When the light-induced temperature goes higher than VPTT, hydrogel inside the pore contracts, it pushes out the chemical stored within hydrogel chains. Conversely, when the temperature falls below the VPTT again, hydrogel columns swell and effectively limit the chemical release. This reversible actuation allows changing the chemical release rate through the designed structure. In addition to the locally controlled release through physically separated pores, the small volume of hydrogel confined within the pore shows rapid actuation compared to other large-sized hydrogels with a slow response time [24-26].

3. Experiments

3.1. Macroporous silicon membrane preparation

Macroporous silicon with 475 μm of pore length was purchased from Smart Membranes, Germany. The backside of a macroporous silicon was lapped using a lapping machine (Buehler Minimet) until pores are open. The lapping process started with mounting the pore side of a macroporous silicon sample on a lapping mount using wax. Next, the sample was lapped using a slurry solution with 1 μm size alumina powders until pores were visible from the bottom of the sample. Then the backside of the sample was polished using slurry solutions with 0.25 μm and 0.1 μm alumina powders respectively to obtain a smooth polished surface. After polishing, the

sample was detached from the lapping mount at 100 °C and cleaned with Opticlear solvent at 80 °C. To further clean all possible contamination inside the pores, 1-hour thermal oxidation was performed at 1100 °C followed by an oxide removal process by buffered oxide etcher. The sample went through additional thermal oxidation for 30 minutes to make a hydrophilic wall inside the pores. The resulting macroporous silicon membrane has a 500 nm thick silicon dioxide layer along the pore walls. The quality of the pore cleanness was checked by observing optical transmission through the pores in a microscope.

3.2. Bulk p-NiPAAm hydrogel preparation

For obtaining about 1 ml thermo-responsive NiPAAm hydrogel solution, 0.2 g of NiPAAm monomer and 0.01 g of BIS crosslinker and 10 µl Darocur 1173 were dissolved in 1 mL Dimethyl sulfoxide (DMSO). The NiPAAm hydrogel solution was cured in a Teflon mold with 1 mm depth under 365nm ultraviolet (UV) illumination for 2 minutes. The polymerized hydrogel was soaked in the deionized (DI) water for one day to replace DMSO with water.

3.3. Bulk graphene-p-NiPAAm hydrogel preparation

Graphene nanoplatelets aggregate was purchased from Alfa Aesar. It is important to disperse graphene nanoplatelets uniformly in DMSO-based NiPAAm hydrogel solution in order to obtain a reliable photothermal effect via graphene nanoplatelets embedded in p-NiPAAm hydrogel. Hydrogel solution was initially prepared by dissolving 4 g of NiPAAm monomer, 0.2 g of BIS crosslinker, and 400 µl Darocur 1173 in 20 mL DMSO. To make 0.01 wt./vol % graphene/NiPAAm (G/NiPAAm) hydrogel solution, 1 mg of graphene nanoplatelets was mixed with 10 mL of the hydrogel solution. To obtain well-dispersed graphene nanoplatelets in the solution, 12 hours of sonication were applied. It was observed that the dispersion quality of the graphene nanoplatelets in hydrogel was significantly improved by 12 hours of sonication as

shown in Figure 2. Different wt./vol % G/NiPAAm hydrogel solutions are prepared accordingly by changing the amount of graphene nanoplatelets mixed in hydrogel solution. To ensure the complete polymerization of G/NiPAAm hydrogel, the curing time was increased to 4 minutes. G/NiPAAm hydrogel solution was UV cured in a circular Teflon mold with 1cm diameter and 1mm depth to form bulk graphene/p-NiPAAm (G/p-NiPAAm) hydrogel.

3.4. G/p-NiPAAm hydrogel in the macroporous silicon membrane

Before filling pores with G/NiPAAm hydrogel solution, the silicon membrane sample was treated with a 3:1 mixture of concentrated sulfuric acid (H_2SO_4) with hydrogen peroxide (H_2O_2) for 10 min to increase hydrophilicity on the surface of the pore walls. After rinsing with DI water, the sample was dried on a 100 °C hot plate for 10 minutes. The sample was mounted in a custom-built Teflon cell, and a few drops of the G/NiPAAm hydrogel solution were placed on the backside of the sample, followed by 10 seconds of cyclic ON/OFF sonication. After the solution filled the pores, it was cured under UV light for its polymerization. After curing hydrogel inside the pores, the glass cover on the backside of the cell was added using four screws. Then DI water was flushed on the sample for a few hours to replace DMSO with water in the cured hydrogel.

4. Result and discussion

4.1. Thermo-responsive characteristics of p-NiPAAm hydrogel

To quantify thermo-responsive characteristics of pure p-NiPAAm hydrogel, bulk p-NiPAAm hydrogel was prepared for optical transmission measurements. At the same time, to facilitate the visualization of the volume change of transparent p-NiPAAm hydrogel, additional hydrogels with 0.1 wt./vol % Sudan II were also prepared. The prepared hydrogel is placed in a

petri-dish with water on a hot plate. While the water temperature is monitored and controlled from 22°C and 47°C, the temperature characteristics of the hydrogel were recorded by a camera. To facilitate the measurement, grid lines of 2mm separation are positioned behind the hydrogel. Figure 3(a) shows the consecutive images of the hydrogel with Sudan II at 22 °C, 35°C, and 47°C. During heating and cooling cycles, the change of the optical transmission through the hydrogel and the size of the hydrogel were measured from consecutive images. Figure 3(b) shows the normalized transmission characteristics of the hydrogel when the cyclic temperature is changed. The measured images are converted to gray-scale images using ImageJ. The normalized optical transmission was extracted from the change of the gray value of the black grid line behind the hydrogel. Figure 3(c) shows the normalized lateral length change of the hydrogel when the cyclic temperature is changed. In addition to the transparency change, the volume of hydrogel decreased when the hydrogel passed the VTPP. As the temperature increased, the volume started to decrease at around 32°C and reached its minimum at 47°C. We also observed that small water droplets appeared from the surface of the hydrogel as the temperature increased at 35°C, which indicates the phase change of the hydrogel from hydrophilic to hydrophobic states, resulting in pushing out the stored liquid from the hydrogel.

4.2. Photothermal response of a bulk G/p-NiPAAm hydrogel

To investigate the photothermal characteristic of G/p-NiPAAm hydrogel, G/p-NiPAAm hydrogels with different graphene concentrations (0, 0.0025, 0.005 wt./vol %) were prepared. Figure 4(a) shows representative images of the prepared hydrogels. All bulk G/p-NiPAAm hydrogels have uniformly dispersed graphene nanoplatelets without aggregation. Figure 4(b) shows the measured spectral absorption of G/p-NiPAAm hydrogel solution with different graphene concentrations before their polymerization. Absorption coefficient (α) was calculated

from the optical transmission measurement by $I = I_o \exp(-\alpha L)$, where I_o is the incident light intensity, I is the measured transmission intensity, and L is the light pass length. Fairly flat absorption characteristics were measured in the spectral domain of 400 nm – 950 nm range. Graphene nanoplatelets increase the absorption coefficient significantly from the base hydrogel solution without them.

Figure 4(c) shows the temperature change of hydrogel as a function of laser illumination time on the prepared hydrogels. For the measurement, a collimated 98mW of near-infrared (NIR) laser at λ=815nm was illuminated on the hydrogel. The beam diameter was measured at around 5.6mm. FLIR i7 compact infrared (IR) thermal imaging camera (FLIR system, USA) was used to measure the temperature at the illumination spot on the hydrogel. The pure p-NiPAAm hydrogel without graphene showed no temperature change during the measurement time window. For other bulk G/p-NiPAAm hydrogels, the temperature increased at the illumination spot with increased illumination time. The temperature increase rate was faster in G/p-NiPAAm hydrogels with a higher concentration of graphene. G/p-NiPAAm hydrogel with 0.0025 wt./vol % graphene was chosen to consider the use of G/p-NiPAAm hydrogel in our macroporous membrane structure. Figure 4(d) shows the photothermal response of 0.0025 wt./vol % G/p-NiPAAm hydrogel as a function of time with different NIR optical power levels. As expected, as the optical illumination power increased, the temperature increment was faster. From the measured absorption as shown in Figure 4(b), 0.0025 wt./vol % graphene will expect to absorb around 23.2% of the illuminated light at 808nm within 1mm thick hydrogel. Based on the measured temperature change per illuminated optical power shown in Figure 4(d), and the absorbed optical power density estimated from the absorption measurement, the conversion

efficiency ($\Delta T/\Delta P$) is estimated to be around 2.87 ºC per 1mW/mm2 after 90 sec of the NIR illumination.

4.3. Photothermal response of G/p-NiPAAm hydrogel columns in a macroporous silicon membrane

To measure the photothermal response of the G/p-NiPAAm hydrogel embedded membrane interface, a custom-built microscope was used with a schematic shown in Figure 5(a). The microscope accommodates conventional fluorescent imaging of fluorescein dye and NIR laser illumination at λ=815nm on the membrane. An additional NIR filter was installed in front of a microscope camera to ensure that NIR illumination is completely blocked on the measured images. White light from the bottom allows measuring the transmission of light through the membrane interface. To monitor the controlled liquid flow through the membrane interface, the membrane was mounted on a 3D printed package. The schematic design and actual image of the mounting package are shown in Figures 4(b) and 4(c). The package allows the membrane to be mounted in a chamber such a way that the top surface of the membrane can be flushed by water, and the bottom of the membrane is in direct contact to 0.2 % fluorescein dye solution in water as a chemical reservoir. 500 μm thick water flushing channel is formed by the membrane surface and a thin glass cover on the top of the package. One side of the channel was connected to an external syringe pump using Tygon tubing to control the flow rate of the surface water flush. The opposite side of the channel is connected to a waste outlet. Figure 6 shows a conceptual schematic of the chemical release by NIR light illumination on the membrane interface.

Figures 6(a) and 6(b) show optical transmission images of white light from the membrane without and with localized NIR laser illumination (marked in the red circle area), respectively. As expected from the photothermal response of G/p-NiPAAm hydrogel, the NIR laser

illumination induces localized temperature increase, where embedded hydrogel turns opaque and blocks the light transmission through the pores, leaving the dark area shown in Figure 7(b). This confirms that hydrogel was successfully embedded within the membrane structure. Figures 6(c) and 6(d) show fluorescent images from the membrane surface without and with localized NIR laser illumination (marked in the red circled area). For this measurement, the bottom white light was turned off, and UV light was illuminated from the top to observe fluorescence from the released fluorescein dye through pores. Since the fluorescein dye is continuously diffused out from the pores of the membrane, the water flush rate on the membrane surface was adjusted to keep track of the released fluorescein dyes without saturating the fluorescent signal in the camera. We found that the water flush rate at 2 ml/min is an optimum condition for our configuration. With this condition, the fluorescent signal on the membrane surface remains constant with an array of visible green spots from the pores. We observed a rapid increase of fluorescent signal in a local area where NIR laser light is illuminated. An example of a photothermal actuation result is also found in a supporting video. This confirms that the proposed design can control the release of chemicals through the membrane interface.

The dynamic control of the liquid release through the membrane interface was investigated by pulsed NIR laser illumination. One set of experiments involved the NIR laser illumination with different power density values tuned to have a series of ON-OFF cycles (one second ON and two second OFF). The illuminated power density was varied from 18.2 mW/mm^2 to 54.6 mW/mm^2 as the videos of fluorescent signals were recorded. The average brightness of the fluorescent signal on the area of NIR illumination was calculated and subtracted from the background signal on the area of no NIR illumination from each frame of the recorded video. Figure 8(a) shows the consecutive fluorescent intensities in the NIR illuminated area,

representing the instant release of fluorescein dyes by a series of cyclic NIR actuation pulses. Increasing the NIR power density demonstrated rapid heating on the hydrogel, which resulted in more contraction of G/p-NiPAAm hydrogel. When the hydrogel contracted more, it is expected that two mechanisms affect the fluorescent signal increase. One is contributed from fluorescein dyes released from the hydrogel, and the other is from the opened channel in the pore, where the contracted hydrogel creates leakage path between pore wall and hydrogel column. Both effects affect the dye release and result in a brighter fluorescent signal. It was observed that the measured fluorescent signal was increased as the laser power density was increased. However, when the structure was modulated with higher optical power, the measured fluorescent signal was gradually decreased as the pulsed actuation was continued. For example, at the power density of 54.6 mW/mm^2, we have observed a noticeable decrease of fluorescent peak intensities compared to the initial pulse actuation. On the contrary, when the actuation was performed with lower peak power, the measured fluorescent peak intensities were fairly consistent over the cyclic pulse actuation. This might be due to the fact that the hydrogel remained contracted before recovering when subsequent optical pulses with higher optical power were applied. Therefore, fluorescein dyes released from the hydrogel are expected to be lower.

Figure 8(b) shows the fluorescent signal intensity for different pulse rates at a fixed NIR optical power of 54.6 mW/mm^2. For this experiment, the laser on-time was fixed, but the laser off-time was varied. At the beginning of the actuations, fluorescent signals were increased during the laser on-time and started to decrease when the laser was off. However, when the next laser pulse was applied before the fluorescent signal was fully decreased, we observed that the fluorescent signal responded to the laser on actuation and was getting brighter. The modulation depth was much smaller for the shorter laser-off case. It is expected that the hydrogel does not

fully recover during this short cooling time and results in a smaller modulation depth. When the laser-off time was increased, the fluorescent signal was gradually decreased and reached to its minimum value with higher modulation depth. While the long-term stability of the hydrogel platform was not studied, there were no physical degradations of the platform observed after the repeated ON/OFF actuation. The hydrogel platform can be used for a prolonged time because the porous silicon membrane is robust and only the functional part of the release system is the top portion of the hydrogel columns which are embedded in pores.

5. Conclusion

We demonstrate the dynamic flow control of fluorescein release through a G/p-NiPAAm hydrogel embedded in an MPS membrane. By dispersing graphene nanoplatelets in p-NiPAAm hydrogel and embedding the hydrogel composite within the pores of the membrane structure, the designed interface structure can control the chemical diffusion rate from the chemical reservoir to the top releasing area remotely by photothermal actuation. Based on the arrayed channel configuration with physical separation, the results show the feasibility of developing a chemical stimulation interface, which requires high spatial resolution to apply target chemicals or drugs with different dose rates. Without physical interconnection, different groups of channels can be remotely and independently controlled by light. Considering the abrupt volume change of p-NiPAAm hydrogel at the narrow temperature range near the VTPP, it is expected to further optimize the release characteristics by adjusting optical absorption through graphene and confining temperature distribution within the pores for higher spatial resolution. This new design mechanism has the potential to create novel chemical-based stimulation devices, which are required in neural prostheses with high spatial resolutions.

Acknowledgment

This work was supported by CUNY PSC-CUNY grant and National Science Foundation grant (NSF-1952469).

References

[1] Cohen R.S., "Cell biology of the synapse in neuroscience in the 21st century: From basic to clinical," Springer New York, pp. 309-349, 2013

[2] B. S. Wilson and M. F. Dorman, "Cochlear implants: current designs and future possibilities," *J. Rehabil. Res. Dev.,* vol. 45, *(5),* pp. 695-730, 2008.

[3] E. Bloch, Y. Luo and L. da Cruz, "Advances in retinal prosthesis systems," *Therapeutic Advances in Ophthalmology,* vol. 11, pp. 2515841418817501, 2019.

[4] S. Shim, K. Eom, J. Jeong and S. J. Kim, "Retinal prosthetic approaches to enhance visual perception for blind patients," *Micromachines,* vol. 11, *(5),* pp. 535, 2020.

[5] A. M. Lozano, N. Lipsman, H. Bergman, P. Brown, S. Chabardes, J. W. Chang, K. Matthews, C. C. McIntyre, T. E. Schlaepfer and M. Schulder, "Deep brain stimulation: current challenges and future directions," *Nature Reviews Neurology,* vol. 15, *(3),* pp. 148-160, 2019.

[6] P. S. Larson, "Deep brain stimulation for movement disorders," *Neurotherapeutics,* vol. 11, *(3),* pp. 465-474, 2014.

[7] M. J. Aebersold, H. Dermutz, L. Demkó, J. F. S. Cogollo, S. Lin, C. Burchert, M. Schneider, D. Ling, C. Forró and H. Han, "Local Chemical Stimulation of Neurons with the Fluidic Force Microscope (FluidFM)," *ChemPhysChem,* vol. 19, *(10),* pp. 1234-1244, 2018.

[8] C. M. Rountree, A. Raghunathan, J. B. Troy and L. Saggere, "Prototype chemical synapse chip for spatially patterned neurotransmitter stimulation of the retina ex vivo," *Microsystems & Nanoengineering,* vol. 3, *(1),* pp. 1-12, 2017.

[9] C. M. Rountree, J. B. Troy and L. Saggere, "Microfluidics-based subretinal chemical neuromodulation of photoreceptor degenerated retinas," *Invest. Ophthalmol. Vis. Sci.,* vol. 59, *(1),* pp. 418-430, 2018.

[10] S. Zibek, B. Hagmeyer, A. Stett and M. Stelzle, "Chemical stimulation of adherent cells by localized application of acetylcholine from a microfluidic system," *Frontiers in Neuroengineering,* vol. 3, pp. 113, 2010.

[11] J. Zhao, X. Liang, H. Cao and T. Tan, "Preparation of injectable hydrogel with near-infrared light response and photo-controlled drug release," *Bioresources and Bioprocessing,* vol. 7, *(1),* pp. 1-13, 2020.

[12] S. Lanzalaco and E. Armelin, "Poly (N-isopropylacrylamide) and copolymers: a review on recent progresses in biomedical applications," *Gels,* vol. 3, *(4),* pp. 36, 2017.

[13] L. Li, Y. He, X. Zheng, L. Yi and W. Nian, "Progress on Preparation of pH/Temperature-Sensitive Intelligent Hydrogels and Applications in Target Transport and Controlled Release of Drugs," *International Journal of Polymer Science,* vol. 2021, 2021.

[14] H. Zhang, J. Li, H. Cui, H. Li and F. Yang, "Forward osmosis using electric-responsive polymer hydrogels as draw agents: Influence of freezing–thawing cycles, voltage, feed solutions on process performance," *Chem. Eng. J.,* vol. 259, pp. 814-819, 2015.

[15] N. Farhoudi, H. Leu, L. B. Laurentius, J. J. Magda, F. Solzbacher and C. F. Reiche, "Smart hydrogel micromechanical resonators with ultrasound readout for biomedical sensing," *ACS Sensors,* vol. 5, *(7),* pp. 1882-1889, 2020.

[16] S. Seo, H. R. Azmand and Y. Song, "A fiber optic sensor platform for smart hydrogel event detection," *Optical Fiber Technology,* vol. 58, pp. 102246, 2020.

[17] G. C. Le Goff, R. L. Srinivas, W. A. Hill and P. S. Doyle, "Hydrogel microparticles for biosensing," *European Polymer Journal,* vol. 72, pp. 386-412, 2015.

[18] Z. Sun, C. Song, C. Wang, Y. Hu and J. Wu, "Hydrogel-based controlled drug delivery for cancer treatment: a review," *Molecular Pharmaceutics,* vol. 17, *(2),* pp. 373-391, 2019.

[19] S. Bandyopadhyay, A. Sharma, M. A. A. Alvi, R. Raju and W. R. Glomm, "A robust method to calculate the volume phase transition temperature (VPTT) for hydrogels and hybrids," *RSC Advances,* vol. 7, *(84),* pp. 53192-53202, 2017.

[20] O. Czakkel, B. Berke and K. László, "Effect of graphene-derivatives on the responsivity of PNIPAM-based thermosensitive nanocomposites–A review," *European Polymer Journal,* vol. 116, pp. 106-116, 2019.

[21] L. Breuer, E. Guthmann, M. J. Schöning, R. Thoelen and T. Wagner, "Light-stimulated hydrogels with incorporated graphene oxide as actuator material for flow control in microfluidic applications," in *Multidisciplinary Digital Publishing Institute Proceedings,* 2017, pp. 524.

[22] E. Wang, M. S. Desai and S. Lee, "Light-controlled graphene-elastin composite hydrogel actuators," *Nano Letters,* vol. 13, *(6),* pp. 2826-2830, 2013.

[23] C. Lo, D. Zhu and H. Jiang, "An infrared-light responsive graphene-oxide incorporated poly (N-isopropylacrylamide) hydrogel nanocomposite," *Soft Matter,* vol. 7, *(12),* pp. 5604-5609, 2011.

[24] R. H. Liu, Q. Yu and D. J. Beebe, "Fabrication and characterization of hydrogel-based microvalves," *J Microelectromech Syst,* vol. 11, *(1),* pp. 45-53, 2002.

[25] M. Lei, A. Baldi, E. Nuxoll, R. A. Siegel and B. Ziaie, "A hydrogel-based implantable micromachined transponder for wireless glucose measurement," *Diabetes Technology & Therapeutics,* vol. 8, *(1),* pp. 112-122, 2006.

[26] K. Deng, C. Bellmann, Y. Fu, M. Rohn, M. Guenther and G. Gerlach, "Miniaturized force-compensated hydrogel-based pH sensors," *Sensors Actuators B: Chem.,* vol. 255, pp. 3495-3504, 2018.

List of Figures

Figure 5. (a) Schematic configuration of the custom-built microscope setup. (b) Schematic design of 3D printed experimental mounting cell. (c) Image of the actual experimental cell with a membrane sample mounted for the measurement.

Figure 6. Conceptual operation of NIR light actuated G/p-NiPAAm hydrogel embedded in a macroporous silicon membrane (a) without and (b) with NIR illumination (Green color particles are fluorescein released from pores)

Figure 7. Comparison images of G/p-NiPAAm-membrane responses wihtout and with NIR illumination. (a) Light transmission image without NIR illumination. (b) Light transmission image with NIR illumination. (c) Fluorescent image without NIR illumination. (d) Fluorescent image with NIR illumination. NIR illuminated area is marked in red circle.

Figure 8. Photothermal responses of G/p-NiPAAm-membrane interface with different NIR on-off cyclic illuminations. (a) Fluorescent signal intensity at the illuminated area vs. time for different illuminated power values with on (1 sec)-off (2 sec) cycles. (b) Fluorescent signal intensity at the illuminated area vs. time for different cyclic illumination at 54.6 mW/mm^2 of optical power density.

Figure 1.

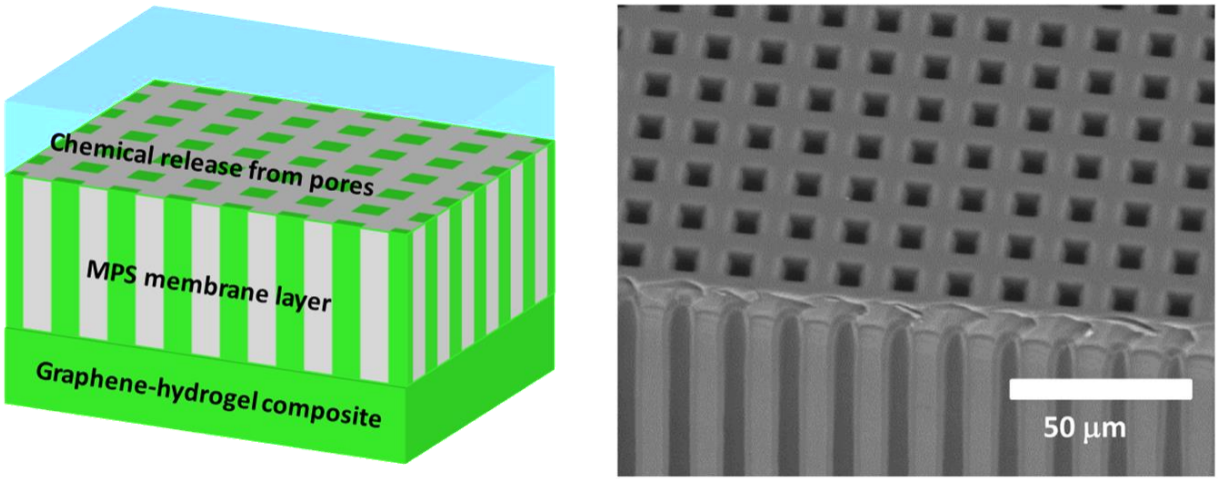
Chemical release from pores
MPS membrane layer
Graphene-hydrogel composite
50 μm

(a) **(b)**

Figure 2.

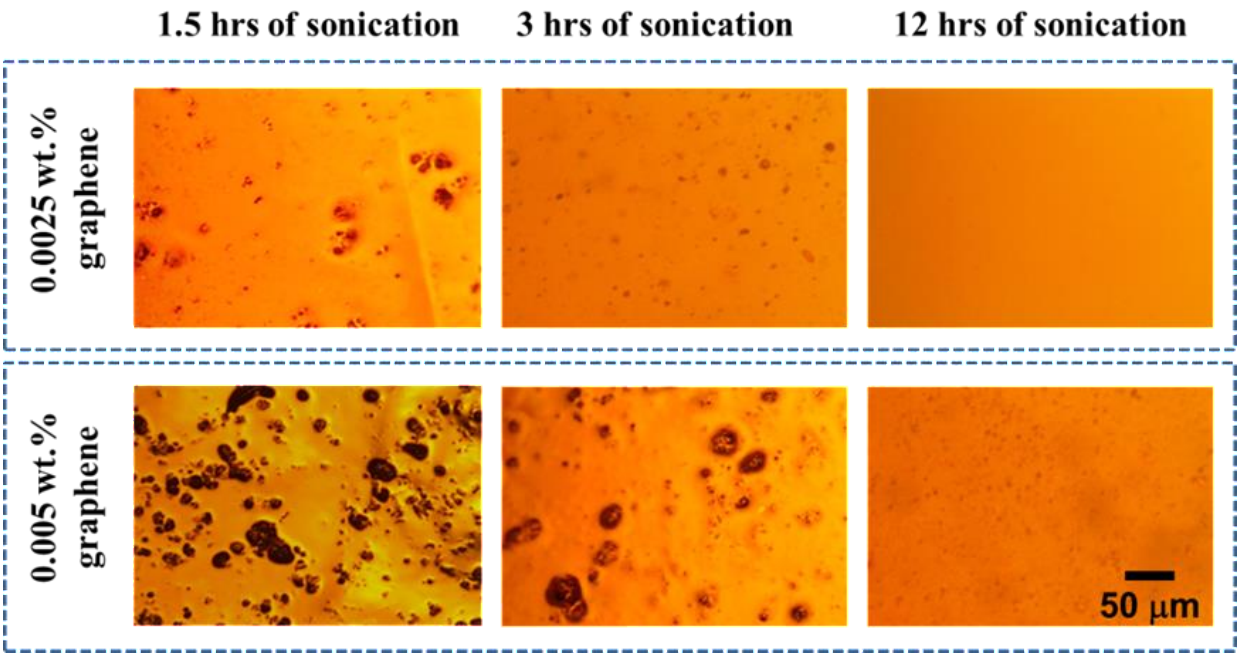
1.5 hrs of sonication
3 hrs of sonication
12 hrs of sonication
0.0025 wt.% graphene
0.005 wt.% graphene
50 μm

Figure 3.

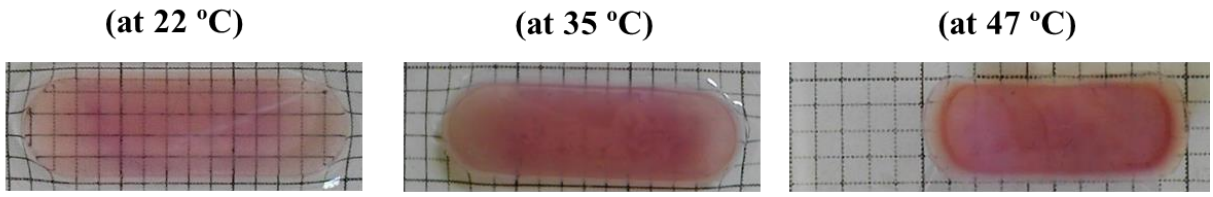
(at 22 ºC)
(at 35 ºC)
(at 47 ºC)

(a)

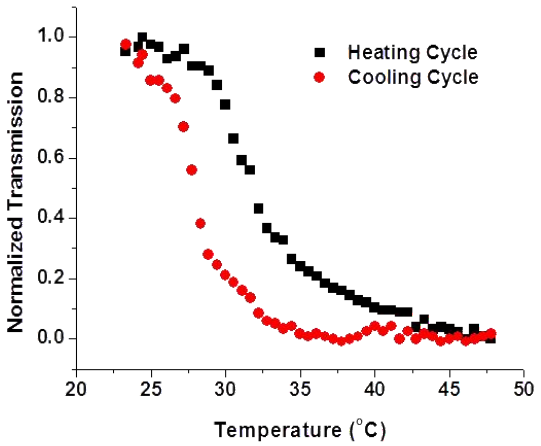
Normalized Transmission
Temperature (°C)
Heating Cycle
Cooling Cycle

(b)

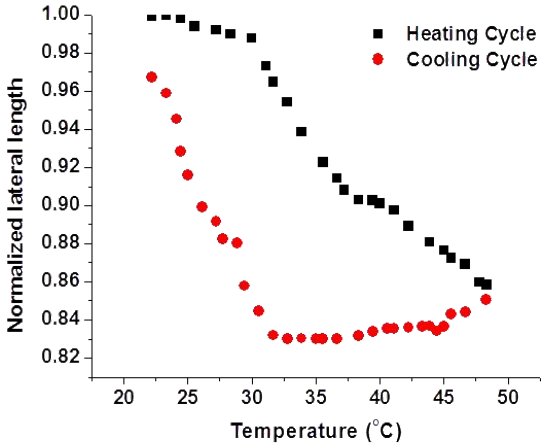
Normalized lateral length
Temperature (°C)
Heating Cycle
Cooling Cycle

(c)

Figure 4.

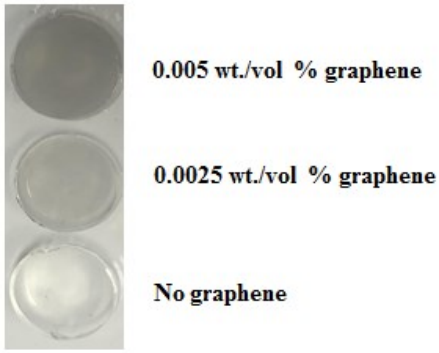

(a)

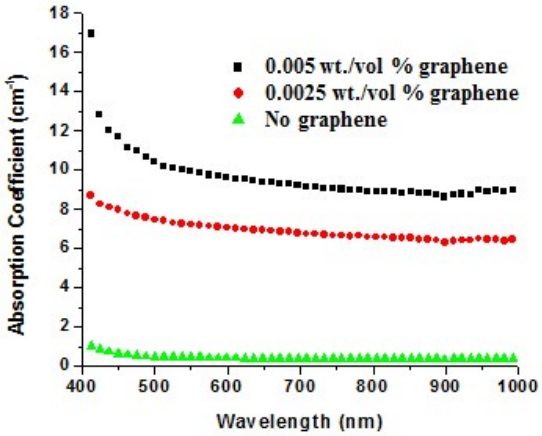

(b)

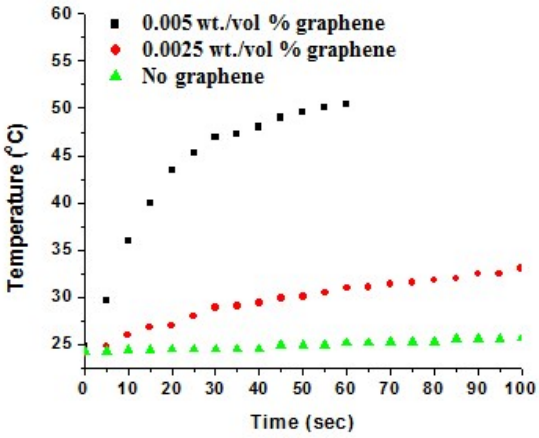

(c)

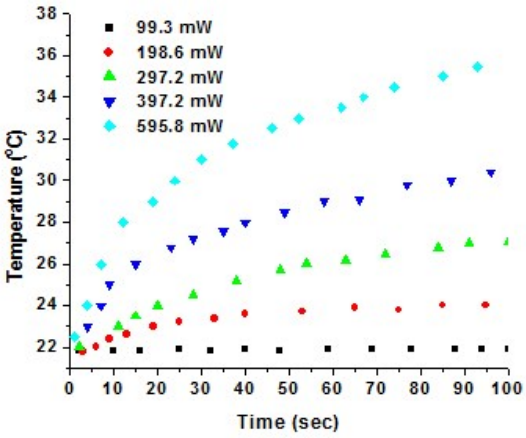

(d)

Figure 5.

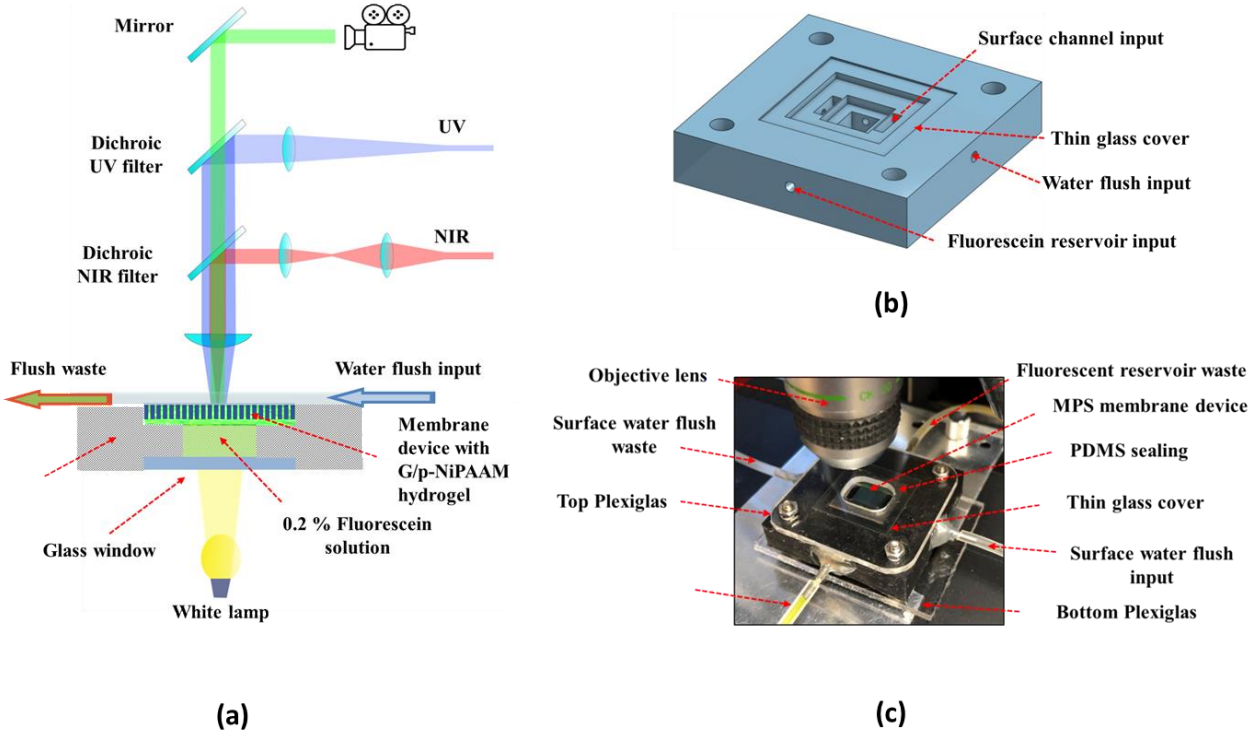
Mirror
UV
Dichroic
UV filter
NIR
Dichroic
NIR filter
Flush waste
Water flush input
Membrane
device with
G/p-NiPAAM
hydrogel
0.2 % Fluorescein
solution
Glass window
White lamp
(a)
Surface channel input
Thin glass cover
Water flush input
Fluorescein reservoir input
(b)
Objective lens
Fluorescent reservoir waste
MPS membrane device
Surface water flush
waste
PDMS sealing
Top Plexiglas
Thin glass cover
Surface water flush
input
Bottom Plexiglas
(c)

Figure 6.

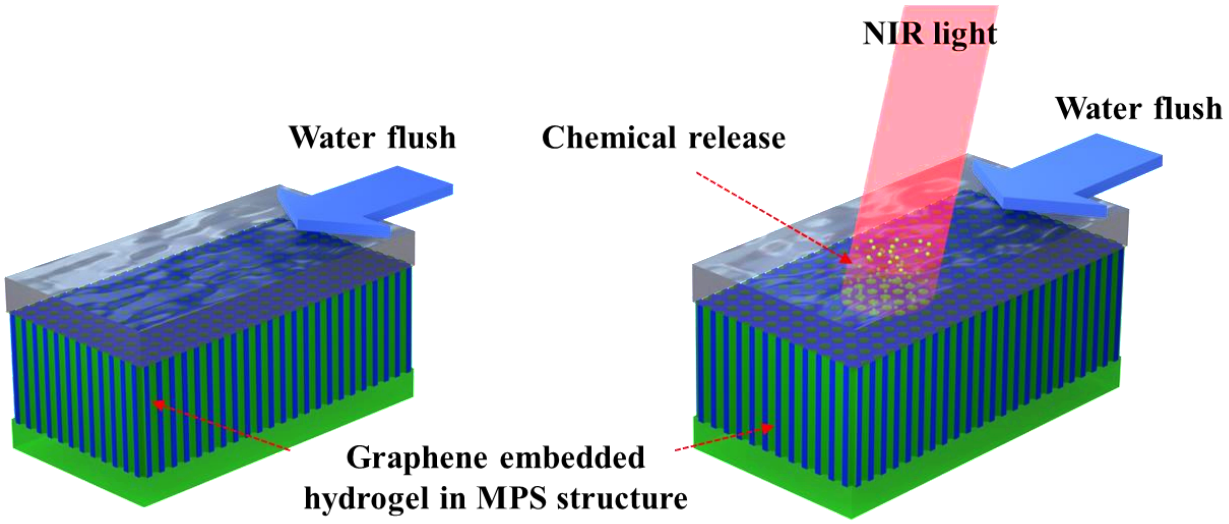
NIR light
Water flush
Water flush
Chemical release
Graphene embedded
hydrogel in MPS structure

Figure 7.

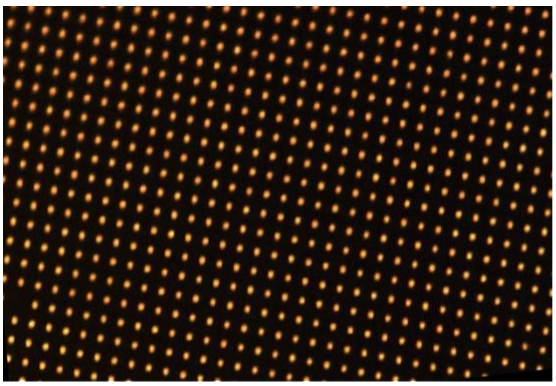

(a)

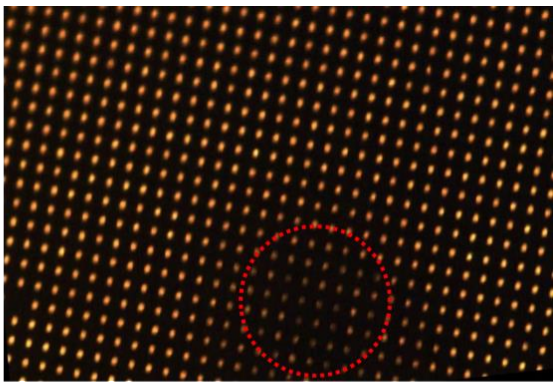

(b)

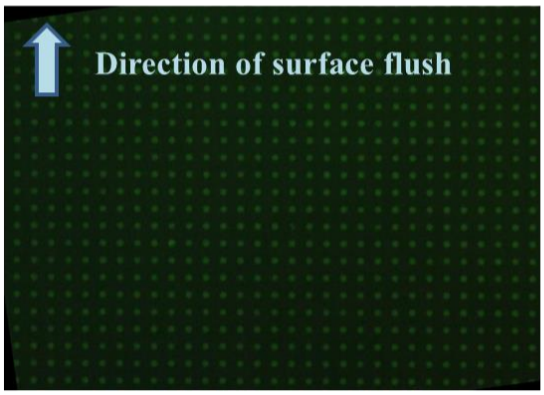

(c)

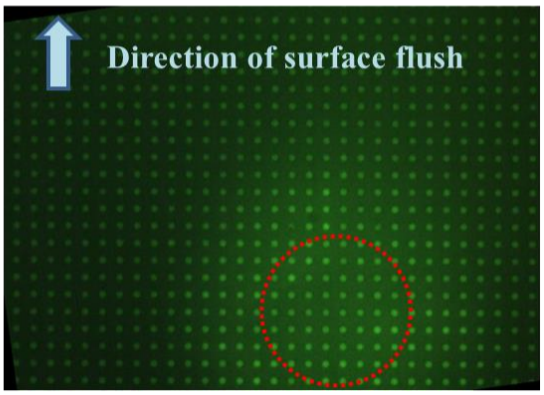

(d)

Figure 8.

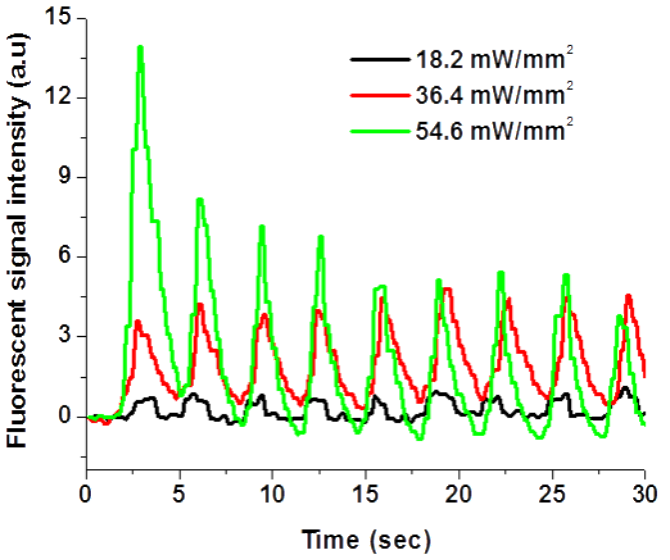
Fluorescent signal intensity (a.u)
Time (sec)
18.2 mW/mm2
36.4 mW/mm2
54.6 mW/mm2
0
3
6
9
12
15
0
5
10
15
20
25
30

(a)

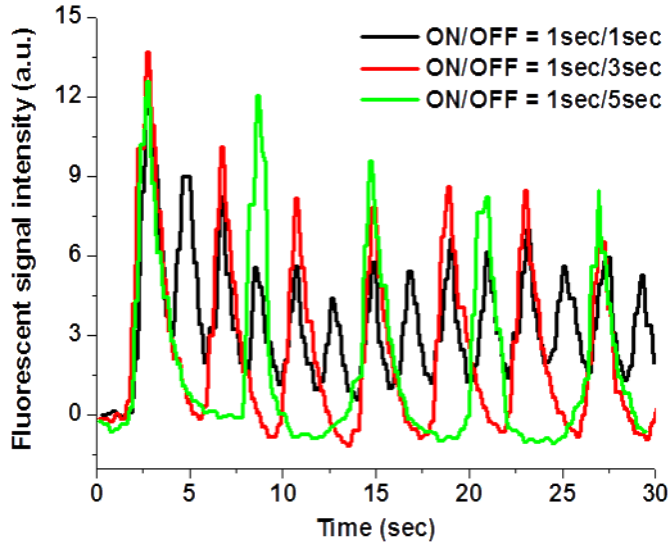
Fluorescent signal intensity (a.u.)
Time (sec)
ON/OFF = 1sec/1sec
ON/OFF = 1sec/3sec
ON/OFF = 1sec/5sec
0
3
6
9
12
15
0
5
10
15
20
25
30

(b)